

Density enhancement mechanism of upwind schemes for low Mach number flows

Bo-Xi Lin¹ · Chao Yan¹ · Shu-Sheng Chen¹

Received: 28 June 2017 / Revised: 8 August 2017 / Accepted: 7 September 2017 / Published online: 2 January 2018

© The Chinese Society of Theoretical and Applied Mechanics; Institute of Mechanics, Chinese Academy of Sciences and Springer-Verlag GmbH Germany, part of Springer Nature 2018

Abstract Many all-speed Roe schemes have been proposed to improve performance in terms of low speeds. Among them, the F-Roe and T-D-Roe schemes have been found to get incorrect density fluctuation in low Mach flows, which is expected to be with the square of Mach number. Asymptotic analysis presents the mechanism of how the density fluctuation problem relates to the incorrect order of terms in the energy equation $\tilde{\rho}\tilde{a}\tilde{U}\Delta U$. It is known that changing the upwind scheme coefficients of the pressure-difference dissipation term D^P and the velocity-difference dissipation term in the momentum equation $D^{\rho U}$ to the order of $O(c^{-1})$ and $O(c^0)$ can improve the level of pressure and velocity accuracy at low speeds. This paper shows that corresponding changes in energy equation can also improve the density accuracy in low speeds. We apply this modification to a recently proposed scheme, TV-MAS, to get a new scheme, TV-MAS2. Unsteady Gresho vortex flow, double shear-layer flow, low Mach number flows over the inviscid cylinder, and NACA0012 airfoil show that energy equation modification in these schemes can obtain the expected square Ma scaling of density fluctuations, which is in good agreement with corresponding asymptotic analysis. Therefore, this density correction is expected to be widely implemented into all-speed compressible flow solvers.

Keywords Energy equation · Density fluctuation · Roe · TV-MAS · Low speeds · All speeds · Computational fluid dynamics

✉ Chao Yan
yanchao@buaa.edu.cn

¹ School of Aeronautic Science and Engineering, Beihang University, Beijing 100183, China

1 Introduction

When with low-speed flow configurations [1–4], numerical schemes developed for compressible flows suffer because the non-physical behavior deteriorates the solution accuracy and because there is a large disparity between the speed of fluid and acoustic wave. There is also a stiffness problem leading to slow calculation. Low-speed preconditioning techniques have been developed to overcome issue of compressible flow solvers in the incompressible limit [5, 6]. Later, the non-physical behavior was demonstrated by asymptotic analysis by Guillard and Viozat in Ref. [7]. As pointed out in the asymptotic analysis, discrete equations of the shock-capturing schemes lead to pressure field P fluctuation with $P(x, t) = P_0(t) + M_* P_1(x, t)$, but the true physical pressure should scale as $P(x, t) = P_0(t) + M_*^2 P_1(x, t)$, where M is the local Mach number, x and t denote space and time.

During recent years, some new attempts to improve the accuracy of conservative schemes in the low-speed limit have been proposed, which focus on dissipation characteristics of flux functions and are different from the previous preconditioning idea. Among the conservative schemes, the Roe scheme [8] is a widely used method for solving compressible flows due to its high resolution for discontinuities and contact shear waves. Many Roe-type schemes with low Mach improvement have been proposed for all speed flows [9]. The work of Li and Gu [10] investigated the joint mechanism of many improved schemes, which include all-speed Roe (A-Roe) [11, 12], Thornber-Drikakis-Roe (T-D-Roe) by Thornber and Drikakis [13], LMRoe by Rieper [14], Fillion-Roe (F-Roe) by Fillion et al. [15]. To construct satisfactory schemes showing the correct asymptotic behavior, Li and Gu [10] found three rules for low speeds through asymptotic theoretical analysis. Based on these disciplines,

improvements for low speeds have been applied to schemes include Harten, Lax, and van Leer (HLL) [10, 16], Roe [17], Toro-Vázquez flux splitting [18]. Another group of popular upwind methods are AUSM-family schemes [19, 20], and their low Mach number modification [21, 22] based on a careful design of dissipation also have been proposed. Besides the accuracy problem, some authors [23, 24] also investigated preconditioned implicit time integration methods for efficient calculation of low-speed flows.

However, the proposed schemes only concern the non-physical behavior of pressure and the checkerboard problem (i.e. correction of pressure and velocity fields), without concerning the correct asymptotic behavior of density field, which is also important as all-speed schemes are mostly applied to density variable flows (low Mach flows [25, 26]) or compressible field with low-speed zones (mixed compressible incompressible flows [27]). In the low Mach number speeds, the pressure field gradually decouples with density as the Mach number decreasing to zero, so the asymptotic density variations of these schemes must also be considered in addition to pressure problems.

The rules for low speed flows developed by Li et al. only concern terms in momentum and continuity equations. In the original T-D-Roe [13] and F-Roe [15] schemes, the energy equation is untouched, while Li and Gu [10] add fixed terms to the energy equation for uniformity, which is just like the form of the momentum equation, and concluded that the modification has little effect on the energy equation. However, it has been found that the correction terms in the energy equation are related closely to the density fluctuation of the flow field in our numerical experiments. These things motivate us to understand the mechanism of density fluctuation with the correction terms in the energy equation and then to find the rules to improve the schemes that have not considered density effects, such as the recently proposed TV-MAS [18].

The outline of this paper is as follows. Section 2 presents the governing equations. Section 3 briefly reviews the Roe, T-D-Roe, F-Roe schemes and the recently proposed TV-MAS method. Their density enhanced versions are also discussed in this section. Section 4 discusses the density fix mechanism with energy equation underlying these schemes and conducts an asymptotic analysis to demonstrate it. The resulting rules of the density fix mechanism are applied to the TV-MAS scheme. Section 5 presents the numerical experiments to support the theoretical analysis and prediction. Finally, Sect. 6 closes the paper with some conclusions.

2 Governing equations

Firstly, the compressible Euler equations in 2D can be written as the following form

$$\frac{\partial \mathbf{q}}{\partial t} + \nabla \cdot \mathbf{F}(\mathbf{q}) = 0, \tag{1}$$

where $\mathbf{F} = (f(q), g(q))$ and is defined as follows

$$\mathbf{q} = \begin{bmatrix} \rho \\ \rho u \\ \rho v \\ \rho E \end{bmatrix}, \quad \mathbf{f} = \begin{bmatrix} \rho u \\ \rho u^2 + p \\ \rho uv \\ \rho uH \end{bmatrix}, \quad \mathbf{g} = \begin{bmatrix} \rho v \\ \rho uv \\ \rho v^2 + p \\ \rho vH \end{bmatrix}, \tag{2}$$

with density ρ , velocity $\mathbf{u} = (u, v)^T$, pressure p , total specific energy $E = e + \frac{1}{2}(u^2 + v^2)$ where internal energy $e = p/\rho(\gamma - 1)$, and total specific enthalpy $H = E + p/\rho$. To close the equations, the perfect gas law is used

$$p = (\gamma - 1) \left[\rho E - \frac{1}{2} \rho (u^2 + v^2) \right], \tag{3}$$

where the specific heat ratio $\gamma = 1.4$.

The finite volume discretization of Eq. (1) can be written as

$$q_{ij}^{n+1} = q_{ij}^n - \frac{\Delta t}{\Omega_{ij}} \sum_{k=1}^{N_f} F_k \Delta S_m, \tag{4}$$

where Ω_{ij} is the 2D finite volume, ΔS_m is the edge length, N_f is the total number of edges composing the finite cell, F_k is the flux function at the edge normal.

3 Review of the schemes

3.1 The original Roe scheme

The original Roe–Pike [8] scheme can be expressed in the following form

$$\mathbf{f}_{c,il}^{\text{Roe}} = \frac{1}{2} (\mathbf{f}_{c,i} + \mathbf{f}_{c,l}) - \frac{1}{2} \mathbf{R} |\mathbf{A}| \alpha_{il}, \tag{5}$$

where \mathbf{R} is the matrix of right eigenvector with the following form

$$\mathbf{R} = \begin{bmatrix} 1 & 1 & 0 & 1 \\ \tilde{u} - n_x \tilde{a} & \tilde{u} & -n_y & \tilde{u} + n_x \tilde{a} \\ \tilde{v} - n_y \tilde{a} & \tilde{v} & n_x & \tilde{v} + n_y \tilde{a} \\ \tilde{H} - \tilde{a} \tilde{U} & \frac{1}{2} (\tilde{u}^2 + \tilde{v}^2) & (n_x \tilde{v} - n_y \tilde{u}) & \tilde{H} + \tilde{a} \tilde{U} \end{bmatrix}, \tag{6}$$

the wave strength α_{il} is defined as

$$\alpha_{il} = \begin{bmatrix} \frac{\Delta p - \tilde{\rho} \tilde{a} \Delta U}{2 \tilde{a}^2} \\ \Delta \rho - \frac{\Delta p}{\tilde{a}^2} \\ \tilde{\rho} \Delta v \\ \frac{\Delta p + \tilde{\rho} \tilde{a} \Delta U}{2 \tilde{a}^2} \end{bmatrix}, \tag{7}$$

where a is the sound speed, $\mathbf{n} = (n_x, n_y)$ is the face normal, $\Delta = ()_i - ()_j$, $\tilde{()}$ means Roe average and the averaged variables are given by

$$\begin{aligned} \tilde{\rho} &= \sqrt{\rho_L \rho_R}, \\ \tilde{\mathbf{u}} &= \frac{\mathbf{u}_L \sqrt{\rho_L} + \mathbf{u}_R \sqrt{\rho_R}}{\sqrt{\rho_L} + \sqrt{\rho_R}}, \\ \tilde{H} &= \frac{H_L \sqrt{\rho_L} + H_R \sqrt{\rho_R}}{\sqrt{\rho_L} + \sqrt{\rho_R}}, \\ \tilde{U} &= \tilde{u} n_x + \tilde{v} n_y, \\ \tilde{q}^2 &= \tilde{u}^2 + \tilde{v}^2, \\ \tilde{a} &= \sqrt{(\gamma - 1)(\tilde{H} - \tilde{q}^2/2)}. \end{aligned} \tag{8}$$

The \mathbf{A} is a diagonal matrix consisting of the relevant eigenvalues:

$$\begin{aligned} \lambda_1 &= \tilde{U} - \tilde{a}, \\ \lambda_2 &= \lambda_3 = \tilde{U}, \\ \lambda_4 &= \tilde{U} + \tilde{a}. \end{aligned} \tag{9}$$

3.2 The F-Roe scheme

Fillion et al. [15] propose a low Mach Roe scheme by adding a pressure correction to the momentum flux as follows

$$f^{\text{F-Roe}} = f^{\text{Roe}} + \frac{1}{2} (1 - f(M)) \begin{pmatrix} 0 \\ \tilde{\rho} \tilde{a} n_x \Delta U \\ \tilde{\rho} \tilde{a} n_y \Delta U \\ 0 \end{pmatrix}, \tag{10}$$

where $f(M)$ is a function of local Mach number and is defined as

$$f(M) = \min(M, 1), \quad M = \max\left(\frac{\sqrt{\mathbf{u}_L^2}}{a_L}, \frac{\sqrt{\mathbf{u}_R^2}}{a_R}\right). \tag{11}$$

This F-Roe scheme is further investigated by Qu et al. [28,29] in supersonic heating problems and Reynolds averaged Navier Stokes (RANS) simulations. There are no energy fix terms in the original F-Roe scheme, and this would result in incorrect density fluctuation which will be shown in asymptotic and numerical experiment. The density correction term is added to energy equation as follows and the scheme is called F-Roe2:

$$f^{\text{F-Roe2}} = f^{\text{Roe}} + \frac{1}{2} (1 - f(M)) \begin{pmatrix} 0 \\ \tilde{\rho} \tilde{a} n_x \Delta U \\ \tilde{\rho} \tilde{a} n_y \Delta U \\ \tilde{\rho} \tilde{a} \tilde{U} \Delta U \end{pmatrix}. \tag{12}$$

3.3 The T-D-Roe scheme

In order to improve the Roe scheme, Thornber and Drikakis [13] modified the right eigenvector as follows

$$\begin{aligned} \mathbf{f}_{c,il}^{\text{T-D-Roe}} &= \frac{1}{2} (\mathbf{f}_{c,i} + \mathbf{f}_{c,l}) - \frac{1}{2} \mathbf{R}^{\text{T-D-Roe}} |\mathbf{A}| \alpha_{il}, \\ \mathbf{R}^{\text{T-D-Roe}} &= \begin{bmatrix} 1 & 1 & 0 & 1 \\ \tilde{u} - n_x \tilde{a}' & \tilde{u} & -n_y & \tilde{u} + n_x \tilde{a}' \\ \tilde{v} - n_y \tilde{a}' & \tilde{v} & n_x & \tilde{v} + n_y \tilde{a}' \\ \tilde{H} - \tilde{a} \tilde{U} & \frac{1}{2} (\tilde{u}^2 + \tilde{v}^2) & (n_x \tilde{v} - n_y \tilde{u}) & \tilde{H} + \tilde{a} \tilde{U} \end{bmatrix}. \end{aligned} \tag{13}$$

The modified acoustic speed \tilde{a}' is scaled by the function $f(M)$

$$\tilde{a}' = \tilde{a} f(M). \tag{15}$$

The T-D-Roe with modified energy equation is as follows

$$\mathbf{R}^{\text{T-D-Roe2}} = \begin{bmatrix} 1 & 1 & 0 & 1 \\ \tilde{u} - n_x \tilde{a}' & \tilde{u} & -n_y & \tilde{u} + n_x \tilde{a}' \\ \tilde{v} - n_y \tilde{a}' & \tilde{v} & n_x & \tilde{v} + n_y \tilde{a}' \\ \tilde{H} - \tilde{a}' \tilde{U} & \frac{1}{2} (\tilde{u}^2 + \tilde{v}^2) & (n_x \tilde{v} - n_y \tilde{u}) & \tilde{H} + \tilde{a}' \tilde{U} \end{bmatrix}. \tag{16}$$

In Eq. (16), the acoustic terms in $\mathbf{R}^{\text{T-D-Roe2}}(4, 1)$ and $\mathbf{R}^{\text{T-D-Roe2}}(4, 4)$ are also scaled by $f(M)$, while in the original T-D-Roe they are the same as Roe scheme.

Through mathematical transformation, the T-D-Roe2 can be written as the form of F-Roe2 as follows

$$f^{\text{T-D-Roe2}} = f^{\text{Roe}} + \frac{1}{2} (1 - f(M)) \begin{pmatrix} 0 \\ \tilde{\rho} \tilde{a} n_x \Delta U + \tilde{U} \frac{\Delta p}{a} n_x \\ \tilde{\rho} \tilde{a} n_y \Delta U + \tilde{U} \frac{\Delta p}{a} n_y \\ \tilde{\rho} \tilde{a} \tilde{U} \Delta U + \tilde{U}^2 \frac{\Delta p}{a} \end{pmatrix}. \tag{17}$$

As we can see from Eq. (17), the T-D-Roe2 has a very similar form of F-Roe2 in Eq. (12), which implies that they may have similar performance at low speeds.

3.4 The TV-MAS scheme

Based on the idea that velocity and pressure should be separately treated owing to the different physics between the convective and acoustic waves, new flux vector splitting (FVS) schemes have been developed. These methods rely on some forms of splitting procedures. Up to now, there mainly exist procedures of Liou-Steffen [19], Zha-Bigen [30], and Toro-Vázquez [31] to split the Euler equations into the *advection system* and *pressure system*. Further discussions and developments for these methods can be found

in Refs. [18,32–34]. The main differences between those splitting procedures lie in the energy equation of the *convective system*: Liou-Steffen’s total enthalpy, Zha-Bigen’s total energy, and Toro-Vázquez’s kinetic energy respectively.

The TV-MAS scheme proposed by Sun et al. [18] based on Toro-Vázquez’s splitting is reviewed here, and the TV-MAS has been claimed as an all-speed scheme in the original paper. In the Toro-Vázquez’s splitting, *advection system* has no pressure terms, and it only appears in *pressure system*, moreover, this splitting allows direct use of Godunov-type methods to the separated system. These characteristics make the splitting procedures attractive.

Following Toro-Vázquez’s splitting, the flux vector of Eq. (1) is split into the *advection system* and *pressure system*:

$$\mathbf{F}(\mathbf{q}) = \mathbf{A}(\mathbf{q}) + \mathbf{P}(\mathbf{q}), \tag{18}$$

where

$$\mathbf{A}(\mathbf{q}) = \begin{pmatrix} \rho \\ \rho u \\ \rho v \\ \rho(u^2 + v^2)/2 \end{pmatrix}, \mathbf{P}(\mathbf{q}) = \begin{pmatrix} 0 \\ n_x p \\ n_y p \\ U(\rho e + p) \end{pmatrix}. \tag{19}$$

The interface numerical flux then can be written as

$$F_{1/2} = \frac{1}{2}(\mathbf{A}_L + \mathbf{A}_R) - \delta \mathbf{A}_{\frac{1}{2}} + \frac{1}{2}(\mathbf{P}_L + \mathbf{P}_R) - \delta \mathbf{P}_{\frac{1}{2}}. \tag{20}$$

The *advection system* is solved by simply upwinding, and the convective dissipation vector is

$$\delta \mathbf{A}_{\frac{1}{2}} = M_k \begin{pmatrix} \rho \\ \rho u \\ \rho v \\ \rho(u^2 + v^2)/2 \end{pmatrix}_k a_k, \tag{21}$$

$$k = \begin{cases} L, & \text{if } \bar{U} \geq 0, \\ R, & \text{if } \bar{U} < 0, \end{cases} \tag{22}$$

where $\bar{U} = (u_L + u_R)/2$ and

$$M_K = \begin{cases} \frac{\bar{U}}{\bar{U} - S_L}, & \bar{U} \geq 0, \\ \frac{\bar{U}}{\bar{U} - S_R}, & \bar{U} < 0, \end{cases} \tag{23}$$

$$a_k = \begin{cases} U_L - S_L, & \bar{U} \geq 0, \\ U_R - S_R, & \bar{U} < 0, \end{cases} \tag{24}$$

$$S_L = \min(0, U_L - a_L, \tilde{U} - \tilde{a}), \tag{25}$$

$$S_R = \min(0, U_R + a_R, \tilde{U} - \tilde{a}). \tag{26}$$

The *pressure system* is dealt with using an HLL-type [35] Riemann solver, and then the authors follow an isotropy

transformation in AUFS scheme [36], and the resulting pressure dissipation vector is written as

$$\delta \mathbf{P}_{\frac{1}{2}} = \frac{S_R + S_L}{2(S_R - S_L)}(\mathbf{P}_R - \mathbf{P}_L) + \frac{S_R + S_L}{(S_R - S_L)\bar{a}^2} \times \begin{pmatrix} p_L - p_R \\ \frac{f(M)[(pu)_L - (pu)_R]}{f(M)[(pv)_L - (pv)_R]} \\ \frac{\bar{a}^2}{(\gamma-1)}(p_L - p_R) + \frac{1}{2}[(p(u^2 + v^2))_L - (p(u^2 + v^2))_R] \end{pmatrix}, \tag{27}$$

where $\bar{a} = \frac{a_L + a_R}{2}$. As we can see, the TV-MAS scheme has applied the rules proposed by Li and Gu [10] to pressure dissipation terms, which modifies the pressure-difference terms in momentum equations by the factor $f(M)$, but apparently the energy equation is neglected by the original authors.

4 Asymptotic analysis

Under the adiabatic compression condition, pressure and density are related to each other as $\frac{p}{\rho^\gamma} = \text{const}$ [37], so the density field would have the same fluctuation pattern as the pressure. To find the mechanism for how the correction term in the energy equation influences density fluctuation, an asymptotic analysis, which has been widely used in Refs. [7,10,11,14], is performed. Previous asymptotic analysis of continuous Euler equation has found that pressure field fluctuates with the square of Mach number, and the asymptotic analysis of the discrete equations with Roe scheme has revealed the terms related to the pressure fluctuation. This time we will find the density related terms in the discrete equations.

Following Ref. [7], the parameters ρ^* , u^* , and a^* are used to normalize the compressible Euler equations, which are defined as $\rho^* = \max(\rho_i(x))$, $u^* = \max(|\mathbf{u}_i(x)|)$, and the acoustic speed $a^* = \sqrt{\gamma \max(p_i(x))/\rho^*}$, where $\rho_i(x)$, $\mathbf{u}_i(x)$, and $p_i(x)$ are the initial values of the discrete domain. The normalized variables are listed in the following form

$$\begin{aligned} \tilde{\rho} &= \frac{\rho}{\rho^*}, \quad \tilde{u} = \frac{u}{u^*}, \quad \tilde{v} = \frac{v}{u^*}, \quad \tilde{p} = \frac{p}{\rho^*(a^*)^2}, \\ \tilde{e} &= \frac{e}{(a^*)^2}, \quad \tilde{x} = \frac{x}{\delta^*}, \quad \tilde{y} = \frac{y}{\delta^*}, \quad \tilde{t} = \frac{tu^*}{\delta^*}, \\ M_* &= u^*/a^*. \end{aligned} \tag{28}$$

Here M_* is the reference Mach number and δ^* is the characteristic mesh element size. Then all normalized variables are asymptotically expanded into powers of the reference Mach number M_*

$$\tilde{\phi} = \tilde{\phi}^{(0)} + M_* \tilde{\phi}^{(1)} + M_*^2 \tilde{\phi}^{(2)} + O(M_*^2), \tag{29}$$

Table 1 Symbols in asymptotics

Symbol	Illustration
$\mathbf{i} = (i, j)$	Index vector for cell
$\mathbf{l} = (i \pm 1, j), (i, j \pm 1)$	Index vector for neighboring cells
\mathbf{il}	Index for the interface between cell i and l
$v(\mathbf{i}) = \{(i \pm 1, j), (i, j \pm 1)\}$	Index set for neighboring cells of cell i
δ_{il}	Mesh size of cell interface il
$\Delta_{\mathbf{il}}(\cdot) = (\cdot)_{\mathbf{i}} - (\cdot)_{\mathbf{l}}$	Difference operator
$\mathbf{n}_{\mathbf{il}} = (n_x, n_y)_{\mathbf{il}}^T$	Unit outer normal vector from cell i to l
$\mathbf{t}_{\mathbf{il}} = (n_x, n_y)_{\mathbf{il}}^T$	Unit transverse vector from cell i to l
$\mathbf{u} = (u, v)^T$	Velocity components with Cartesian coordinates
$U = \mathbf{u} \cdot \mathbf{n} = un_x + vn_y$	Normal component of velocity vector \mathbf{u}

where $\tilde{\phi}$ represents all the physical variables ($\tilde{\rho}, \tilde{u}, \tilde{v}, \tilde{p}, \tilde{e}$) respectively. In the following sections, we will drop the tilde \sim for convenience and all the symbols used in analysis are presented in Table 1.

Inserting the asymptotic expansion Eq. (29) into the F-Roe scheme, we collect terms with the same power of M_* . In Ref. [14], Rieper has analyzed the terms with the order of $1/M_*^2, 1/M_*$, and M_*^0 , and has found the mechanisms to get the correct pressure field. This correction also fixes the Mach contours of the flows. However, the pressure has a limited influence on density in low Mach number. So further analysis must be conducted upon the asymptotic expansion of pressure to find the density enhance mechanism. We gather the terms with order M_*^1 in continuity and energy equations as follows

continuity equation:

$$\begin{aligned} & \frac{1}{2} \sum_{l \in v(i)} \rho_{il}^{(0)} \frac{U_{il}^{(0)}}{a_{il}^{(0)}} \Delta_{il} U^{(0)} \delta_{il} + A_i \frac{d}{dt} \rho_i^{(1)} \\ & + \frac{1}{2} \sum_{l \in v(i)} \left\{ pg \frac{\Delta_{il} p^{(2)}}{a_{il}^{(0)}} + (\rho_l u_l)^{(1)} \cdot n_{il} \right. \\ & \left. + \left[(|U_{il}| \Delta_{il} \rho)^{(1)} - \frac{(|U_{il}| \Delta_{il} p)^{(1)}}{(a_{il}^{(0)})^2} \right] \right\} \delta_{il} = 0, \quad (30) \end{aligned}$$

energy equation:

$$\begin{aligned} & \frac{1}{2} \sum_{l \in v(i)} \left[\left(\frac{U_{il}^2}{a_{il}^{(0)}} \Delta_{il} p^{(0)} \right) + \rho_{il}^{(0)} a_{il}^{(0)} U_{il}^{(0)} \Delta_{il} U^{(0)} \right. \\ & \left. + \rho_{il}^{(0)} \frac{U_{il}^{(0)}}{a_{il}^{(0)}} h_{il}^{(0)} \Delta_{il} U^{(0)} \right] \delta_{il} \end{aligned}$$

$$\begin{aligned} & + A_i \frac{d}{dt} (\rho_i e_i)^{(1)} + \frac{1}{2} \sum_{l \in v(i)} \left\{ \frac{[h_{il} \Delta_{il} p]^{(2)}}{a_{il}^{(0)}} \right. \\ & \left. + [(\rho_l e_l u_l)^{(1)} + (p_l u_l)^{(1)}] \cdot n_{il} \right\} \delta_{il} = 0. \quad (31) \end{aligned}$$

According to the analysis of terms with $1/M_*^2, 1/M_*$, and M_*^0 , the following results hold

$$\begin{aligned} & \rho^{(0)} = \text{const}, \\ & p^{(0)} = \text{const}, \\ & p^{(1)} = \text{const}, \\ & \nabla \cdot \mathbf{u}^{(0)} = \mathbf{0}. \quad (32) \end{aligned}$$

Let Eq. (30) multiply $h_{il}^{(0)}$ and subtract with Eq. (31), getting the equation

$$\begin{aligned} & \frac{1}{2} \sum_{l \in v(i)} \rho_{il}^{(0)} a_{il}^{(0)} U_{il}^{(0)} \Delta_{il} U^{(0)} \delta_{il} \\ & + A_i \frac{d}{dt} (\rho_i e_i)^{(1)} - A_i \frac{d}{dt} \rho_i^{(1)} h_{il}^{(0)} \\ & + \frac{1}{2} \sum_{l \in v(i)} \left[\frac{\gamma p^{(0)}}{\gamma - 1} u_l^{(1)} \cdot n_{il} - \rho_l^{(0)} h_{il}^{(0)} u_l^{(1)} \cdot n_{il} \right. \\ & \left. - |U_{il}|^{(0)} \Delta_{il} \rho^{(1)} h_{il}^{(0)} \right] \delta_{il} = 0. \quad (33) \end{aligned}$$

Using the energy asymptotic equation [14]

$$(\rho e)^{(1)} = \frac{p^{(1)}}{\gamma - 1}, \quad h^{(0)} = \frac{\gamma}{\gamma - 1} \frac{p^{(0)}}{\rho^{(0)}}. \quad (34)$$

Equation (33) can be simplified as

$$\begin{aligned} A_i h_{il}^{(0)} \frac{d}{dt} \rho_i^{(1)} + R &= \frac{1}{2} \sum_{l \in v(i)} \frac{\rho_{il}^{(0)} a_{il}^{(0)} U_{il}^{(0)} \Delta_{il} U^{(0)}}{\rho^{(0)}} \delta_{il}, \\ R &= \frac{1}{2} \sum_{l \in v(i)} \{ |U_{il}|^{(0)} h_{il}^{(0)} \Delta_{il} \rho^{(1)} \} \delta_{il}. \quad (35) \end{aligned}$$

Note that for a simple entropy conservative shear flow with constant density and pressure, R only has the transport term for $\rho^{(1)}$. An excessive damping of the $\rho^{(1)}$ origins from the underline term in Eq. (35). In the F-Roe2 and T-D-Roe2 schemes, this term is lifted with the $f(M)$ function ($\Delta_{il} U^{(0)} \rightarrow 0$), and reduces the artificial viscosity to the correct level. This density correction effects will be shown in the following numerical experiments.

That is to say, fix terms also should be applied to the energy equation to get the right density fluctuation, based

on the pressure fix added to momentum equations. The non-physical phenomenon of upwind schemes at low speed can be cured following the rules of Li and Gu [10], and now we have shown that extra fix terms in the energy equation needed to be considered based on a similar form of momentum correction. According to this theory, we propose the TV-MAS2 scheme, which fixes the energy equation with the $f(M)$ function upon the original TV-MAS scheme. In order to get the correct density fluctuation, the energy equation in $\delta \mathbf{P}_{\frac{1}{2}}$ is modified as the way in momentum equations, resulting the following TV-MAS2 scheme

$$\delta \mathbf{P}_{\frac{1}{2}} = \frac{S_R + S_L}{2(S_R - S_L)}(\mathbf{P}_R - \mathbf{P}_L) + \frac{S_R + S_L}{(S_R - S_L)\bar{a}^2} \times \begin{pmatrix} p_L - p_R \\ f(M)[(pu)_L - (pu)_R] \\ f(M)[(pv)_L - (pv)_R] \\ \frac{\bar{a}^2}{(\gamma-1)}(p_L - p_R) + \frac{1}{2}f(M)[(p(u^2+v^2))_L - (p(u^2+v^2))_R] \end{pmatrix} \tag{36}$$

5 Numerical results

5.1 Gresho vortex

In their work, Gresho and Chan [38,39] proposed a time-independent solid body rotating vortex flow. In this unsteady moving flow, the vortex can be transported without distortion by the background flow. We choose a computation domain of $[0, 1] \times [0, 1]$, and periodic conditions are applied on the horizontal direction, while characteristic conditions are on the vertical edges. The domain is first initialized with a uniform background flow of density ρ_0 , pressure P_0 , and given Mach M_0 as follows

$$\begin{aligned} \rho_0 &= 1.0, \quad \mathbf{u}_0 = (u_0, 0)^T, \quad p_0 = 1.0, \\ c_0 &= \sqrt{\gamma p_0 / \rho_0} = \sqrt{\gamma}, \quad u_0 = M_0 c_0. \end{aligned} \tag{37}$$

A perturbed initial condition permitting different Mach numbers is proposed in Ref. [14]. At the time $t = 0$ of the perturbed flow, a vortex is located at $(x_0, y_0) = (0.5, 0.5)$ with the radius $R = 0.4$. At the position $r = R$, the vortex tangential velocity decreases to zero. This perturbed vortex is added to the background flow as follows

$$u_r(r) = u_0 \begin{cases} 2r/R, & \text{if } 0 \leq r < R/2, \\ 2(1-r/R), & \text{if } R/2 \leq r < R, \\ 0, & \text{if } R \leq r, \end{cases} \tag{38}$$

$$p(r) = p_0 + u_0^2 \begin{cases} 2r^2/R^2 + 2 - \log 16, & 0 \leq r < R/2, \\ 2r^2/R^2 - 8r/R + 4 \log(r/R), & R/2 \leq r < R, \\ 0, & R \leq r, \end{cases} \tag{39}$$

$$r = \sqrt{(x - x_0)^2 + (y - y_0)^2}, \tag{40}$$

where the $u_r(r)$ denotes the radial velocity and we obtain the Cartesian components by

$$\begin{aligned} u(x, y) &= u_0 - \frac{y - y_0}{r} u_r(x, y), \\ v(x, y) &= \frac{x - x_0}{r} u_r(x, y). \end{aligned} \tag{41}$$

According to the initial condition, the pressure field has the following fluctuation relation

$$p = p_0 + u_0^2 p^{(2)}. \tag{42}$$

The original incompressible test case is extended to a weakly compressible one by introducing the adiabatic compression $p = \rho^\gamma$, which makes the initial density field have a similar form to pressure fluctuations

$$\rho = \rho_0 + u_0^2 \rho^{(2)}. \tag{43}$$

We use a Cartesian grid of $[120 \times 120]$, and all simulations are run until one domain passage is reached. The strong stability preserving a three-stage third-order Runge-Kutta (SSP-RK3) [40] scheme is used for temporal discretization.

In Ref. [9], the evolution of a normalized pressure field $\tilde{p}_f \in [0, 1]$ is used to characterize the accuracy of the computations in incompressible limit. The normalized pressure field \tilde{p}_f is expressed as

$$\tilde{p}_f(\mathbf{x}) = \frac{p(x) - p_{\min}}{p_{\max} - p_{\min}}, \tag{44}$$

where p_{\min} represents the minimum static pressure in the flow field, and p_{\max} is the maximum. We define similar normalized density field as

$$\tilde{\rho}_f(\mathbf{x}) = \frac{\rho(x) - \rho_{\min}}{\rho_{\max} - \rho_{\min}}. \tag{45}$$

In the Gresho vortex test case, the normalized pressure and density field should be unchanged during transportation independent of initial Mach number. Thus, we use this to evaluate the quality of different schemes in the simulation of Gresho vortex.

Figure 1 shows the normalized pressure fluctuation field of the Gresho vortex for $Ma = 0.1$. Figure 2 shows the corresponding normalized density fluctuation field. As we can see, the original Roe scheme holds the initial maximum P_f of 50%–60% after one domain passage due to the strong dissipation; on the contrary, all others plotted in the figures have preserved the original maximum P_f . All the improved schemes (T-D-Roe, F-Roe, TV-MAS, T-D-Roe2, F-Roe2, TV-MAS2) have achieved the same contour on P_f as F-Roe, thus not all of them are plotted in the figure. However, the difference lies in the density field. Schemes in the

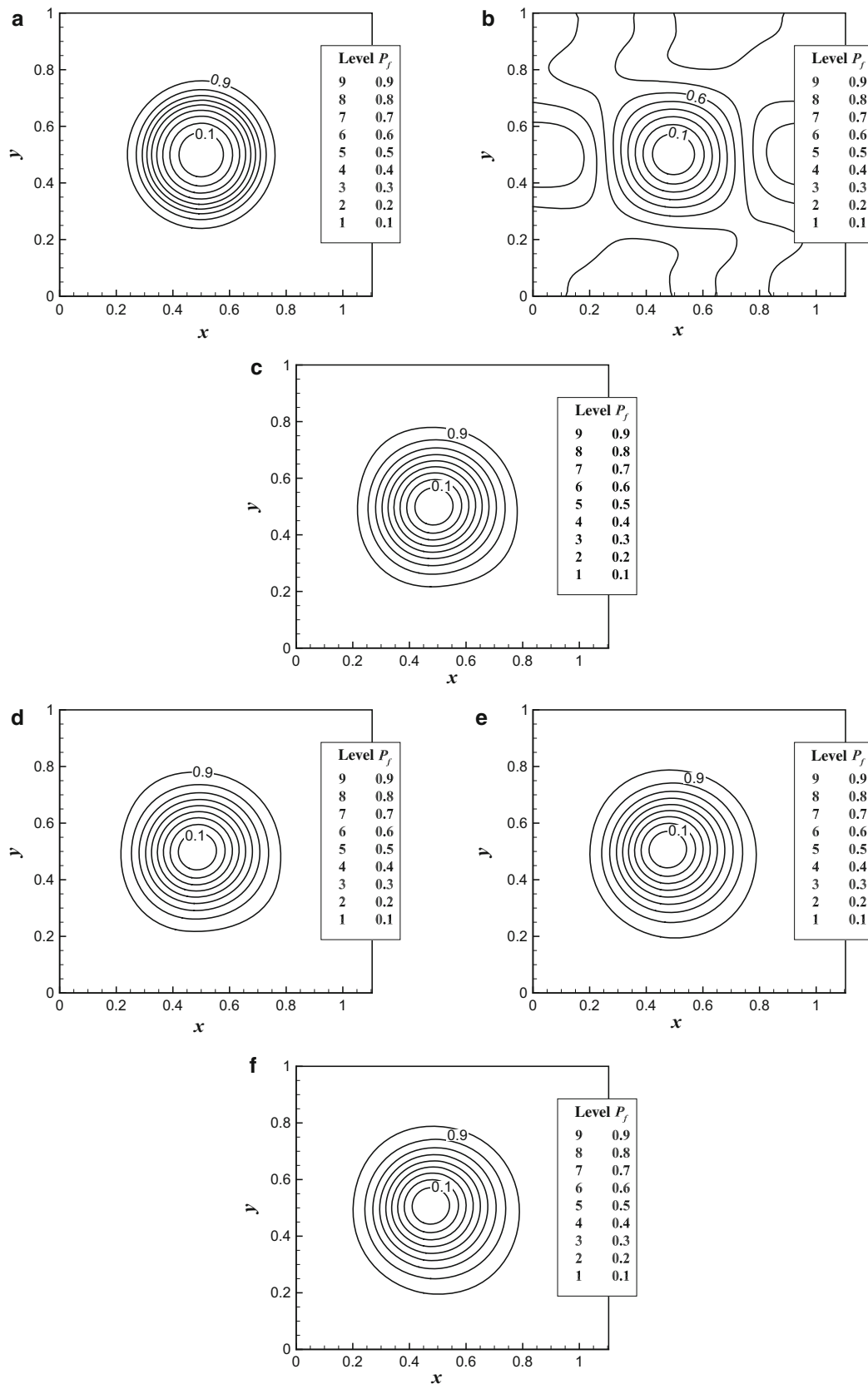


Fig. 1 Normalized pressure field for simulations of a Gresho vortex. **a** Initial pressure field. **b** Roe scheme for $Ma_0 = 0.1$. **c** F-Roe scheme for $Ma_0 = 0.1$. **d** F-Roe2 scheme for $Ma_0 = 0.1$. **e** TV-MAS scheme for $Ma_0 = 0.1$. **f** TV-MAS2 scheme for $Ma_0 = 0.1$

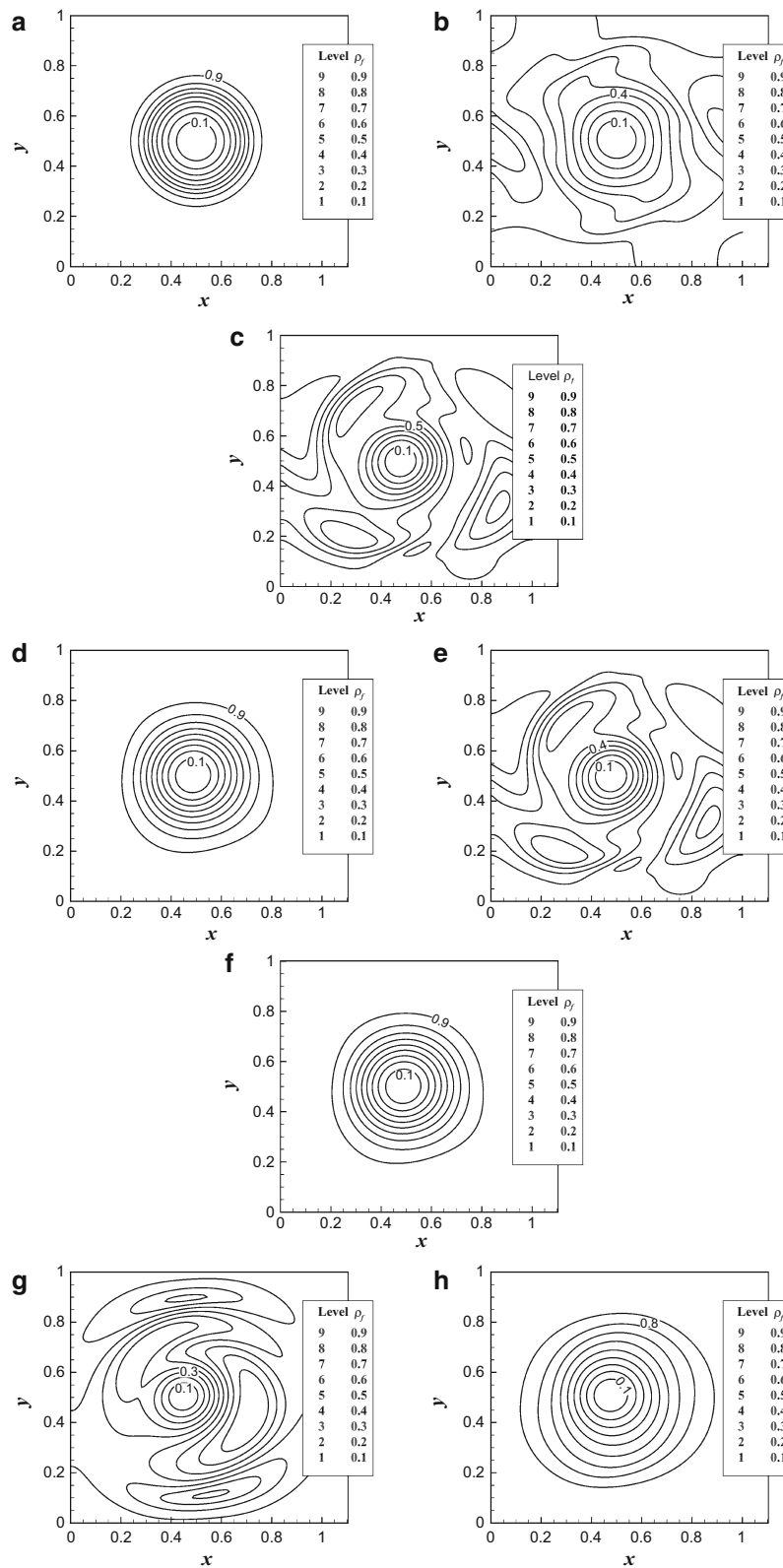


Fig. 2 Normalized density field for simulations of a Gresho vortex. **a** Initial density filed. **b** Roe scheme for $Ma_0 = 0.1$. **c** F-Roe scheme for $Ma_0 = 0.1$. **d** F-Roe2 scheme for $Ma_0 = 0.1$. **e** T-D-Roe scheme for $Ma_0 = 0.1$. **f** T-D-Roe2 scheme for $Ma_0 = 0.1$. **g** TV-MAS scheme for $Ma_0 = 0.1$. **h** TV-MAS2 scheme for $Ma_0 = 0.1$

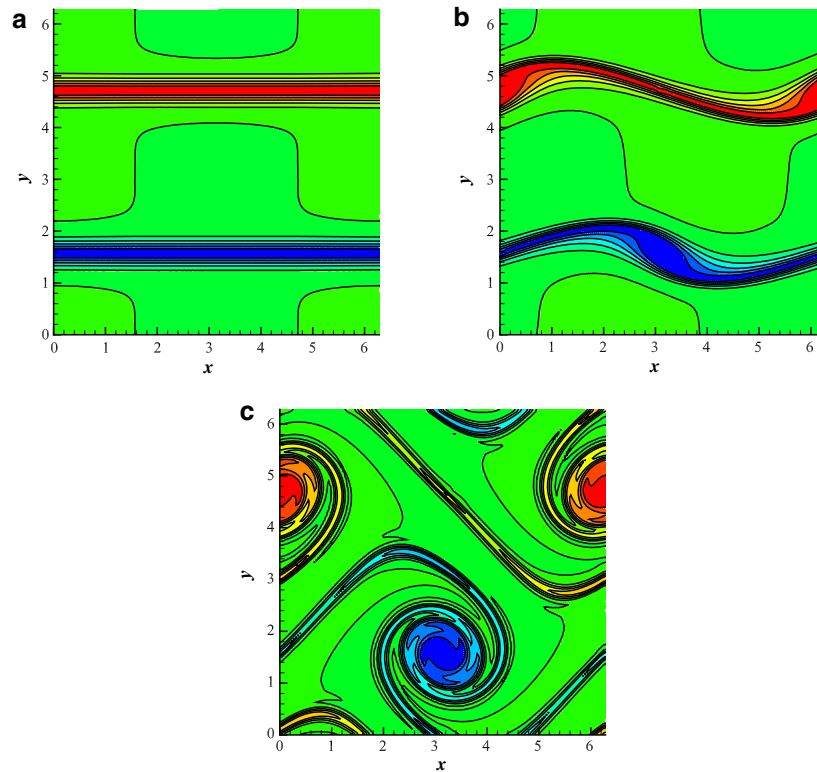


Fig. 3 Vorticity contours of double shear-layer by F-Roe2 schemes at Mach 0.01. **a** $t = 0$. **b** $t = 4.0$. **c** $t = 8.0$

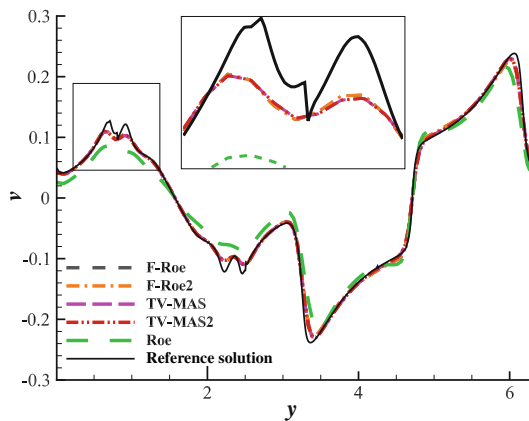


Fig. 4 Velocity v profiles along $x = \pi$ at $t = 8.0$ of double shear layer cases

group with no energy correction (T-D-Roe, F-Roe, TV-MAS) show excessive dissipation to density fluctuation. The original Roe preserves 30% of the maximum ρ_f after one domain passage, while F-Roe is 40%, TV-MAS is 20%. The schemes with energy fix terms (T-D-Roe2, F-Roe2, TV-MAS2) have almost constant density fluctuation as the initial field. This shows the importance of the energy equation fix to get the correct density field in low Mach speeds.

The T-D-Roe series have similar formulas and numerical results as corresponding schemes in F-Roe series, and that

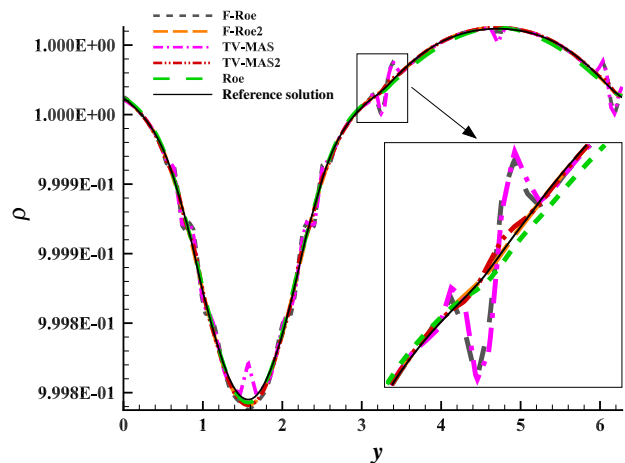


Fig. 5 Density profiles along $x = \pi$ at $t = 8.0$ of double shear layer cases

is verified in the following numerical examples. So in some sections, only the F-Roe results are listed in the discussion.

5.2 Double shear-layer

The “double shear-layer” problem is a typical 2D unsteady inviscid flow. We mostly follow the setup of Ishiko et al. [41] and Kitamura and Hashimoto [42], which makes this problem a weakly compressible flow. Initially, two shear layers are

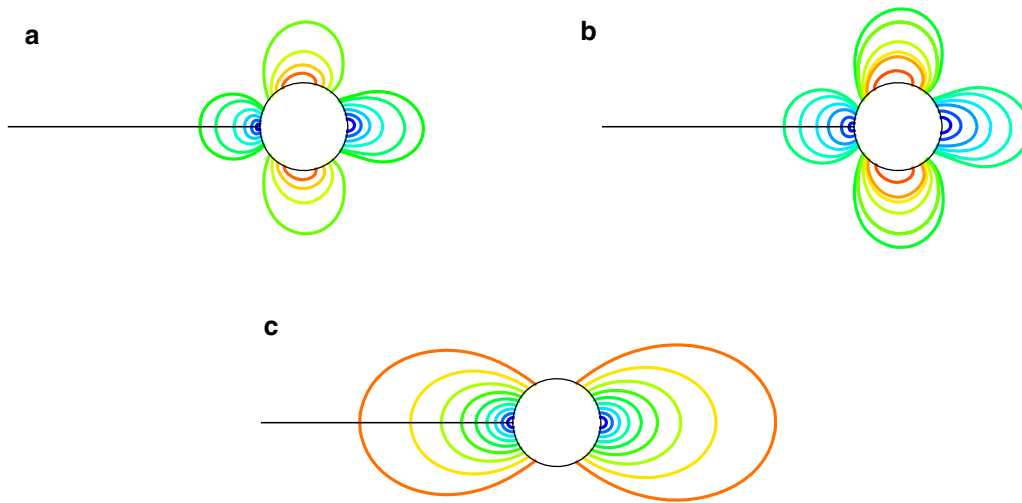


Fig. 6 Mach contours for simulations of flow around inviscid cylinder at Mach 0.001. **a** TV-MAS scheme. **b** TV-MAS2 scheme. **c** Roe scheme

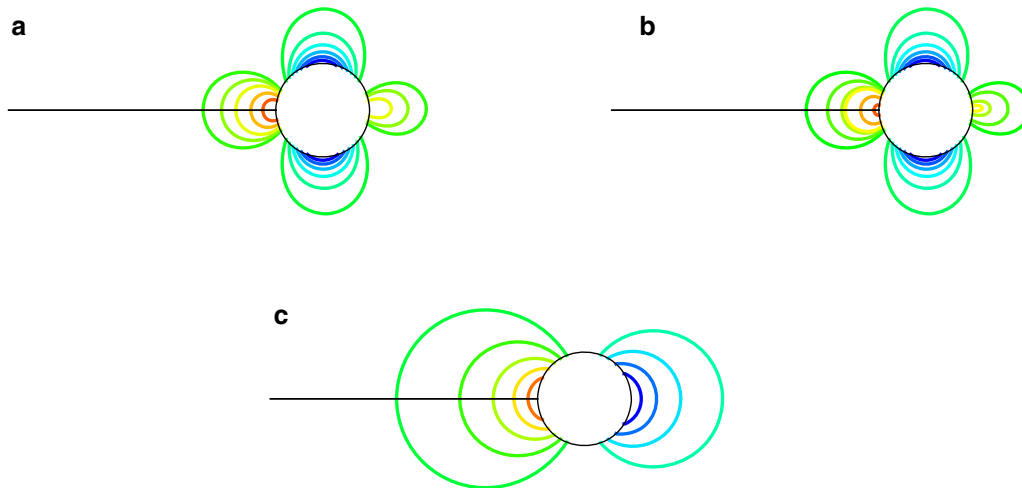


Fig. 7 Pressure contours for simulations of flow around inviscid cylinder at Mach 0.001. **a** TV-MAS scheme. **b** TV-MAS2 scheme. **c** Roe scheme

generated by fluids with opposite velocity (Fig. 3a), then as time progresses, the initial layers will gradually roll up and develop a strong vortical flow structure (Fig. 3b, c) [42]. This vortical structure developed by shear-layer is very different to Gresho’s vortex flow, which possesses a consistent pattern. Thus, we conduct it to highlight further the characteristics of density correction.

The initial conditions for velocity components are

$$u(x, y) = \begin{cases} U_\infty \tanh[(y - \pi/2)/\delta_1], & y \leq \pi, \\ U_\infty \tanh[(3\pi/2 - y)/\delta_1], & y > \pi, \end{cases} \quad (46)$$

$$v(x, y) = \delta_2 \sin(x), \quad (47)$$

where $U_\infty = 1.0$, $\delta_1 = \pi/15$, $\delta_2 = 0.05$. The density is set to be $\rho = 1.0$ and the pressure is chosen to satisfy a Mach number of $M_\infty = 0.01$ with $p = 1/(\gamma M_\infty^2)$. The computational domain is $[0, 2\pi] \times [0, 2\pi]$ and consists of

128^2 grid cells. A periodic boundary condition is adopted at all directions of the computational domain. The simulations are run up to $t = 8.0$ with the SSP-RK3 time scheme at a time step of $\delta t = 5.0 \times 10^{-5}$. The reference solution is achieved with Roe scheme at a very fine grid of 512^2 cells. “At this level of resolution, the flux functions have no influence on the results” [42].

The differences of all simulated schemes are compared in Fig. 4, in which velocity v profiles are listed along $x = \pi$ slice. In Fig. 5, the density profiles along $x = \pi$ are plotted. As we can see from Fig. 4, all the low-Mach enhanced schemes get a more precise velocity v profile than the original Roe, and there are marginal differences among themselves. This proves that the momentum fix can recover the velocity and pressure profile at low Mach limit. However, in Fig. 5, the density profile is very different. The F-Roe and TV-MAS have density jump glitches at the position of strong shear

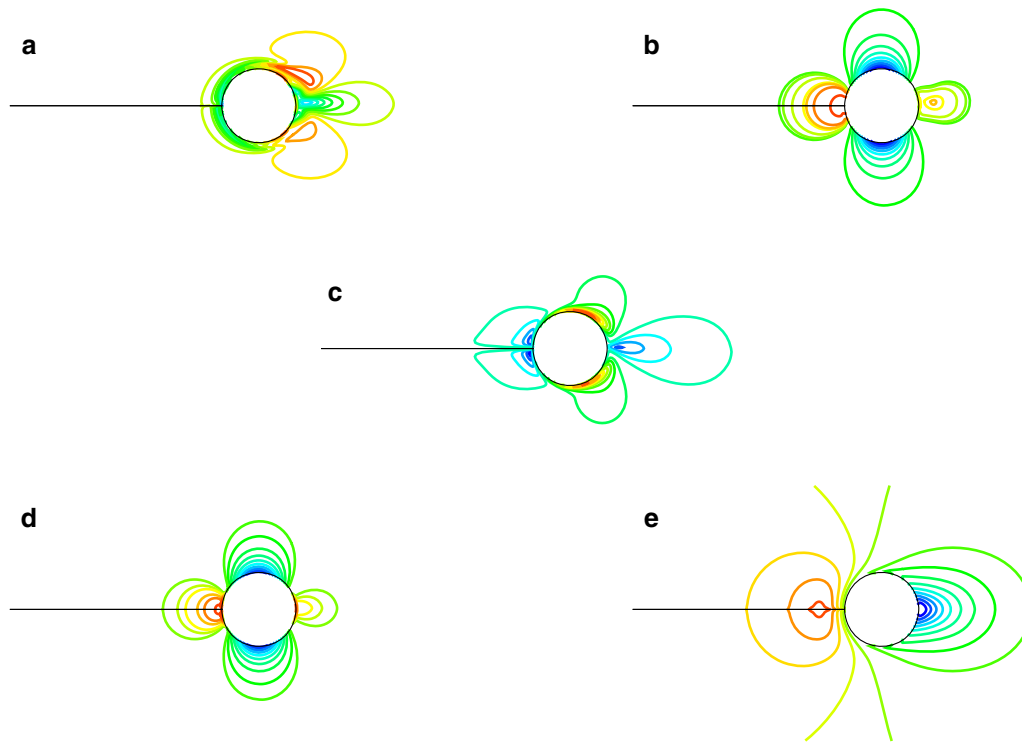


Fig. 8 Density contours for simulations of flow around inviscid cylinder at $Ma = 0.001$. **a** F-Roe scheme. **b** F-Roe2 scheme. **c** TV-MAS scheme. **d** TV-MAS2 scheme. **e** Roe scheme

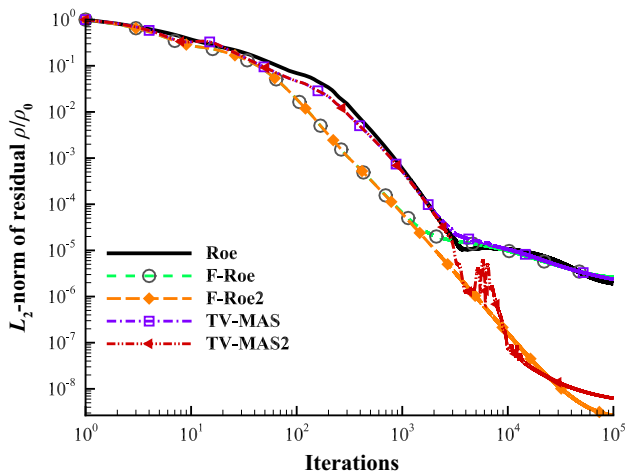


Fig. 9 Convergence comparison of NACA0012 test case at $Ma = 0.01$

effect, while the fixed F-Roe2 and TV-MAS2 can recover correct density profile compared to the reference solution.

5.3 Inviscid cylinder

The Euler flow over a two-dimensional cylinder is a typical low speed flow of blunt body. In this case, the size of the computational domain is $\Omega = [r_0, r_1] \times [\phi_0, \phi_1]$, which is $[0.5, 20] \times [0, 2\pi]$ in details, where r_0 is the radius of a

cylinder surface and r_1 is the radius of exterior boundary. The adopted mesh is O-type and contains 301 (circumference) \times 401 (radius) grid points. The inflow Mach numbers $M_{inf} = 0.001$ with initial conditions of $\rho = 1.0, p = 1/(\gamma M_\infty^2)$. The farfield condition is used at the outer boundary, and the slip wall condition is applied at the cylinder wall.

Figure 6 shows the Mach contours of the TV-MAS, TV-MAS2, and Roe schemes, while Fig. 7 shows the pressure contours. As we can see, in this condition, the TV-MAS and TV-MAS2 get the physical Mach and pressure field, while the original Roe scheme gets nonphysical contours. The T-D-Roe and F-Roe series have the same Mach and pressure results, so are not plotted here. In Refs. [10, 18], it has been shown that the Mach and pressure fields can be solved by the momentum corrections together, so only the pressure fields are used for comparison in the following. Figure 8 shows the density contours of the F-Roe, F-Roe2, TV-MAS, TV-MAS2, and Roe schemes. The Roe, F-Roe, and TV-MAS get diffusive density field, while the TV-MAS2 and F-Roe2 can recover the correct density field. It also can be noticed that the F-Roe and TV-MAS get more diffusive density field than original Roe scheme.

5.4 Inviscid NACA0012 airfoil

The inviscid flow over NACA0012 airfoil is a typical test case at the low-speed condition. An O-type mesh that con-

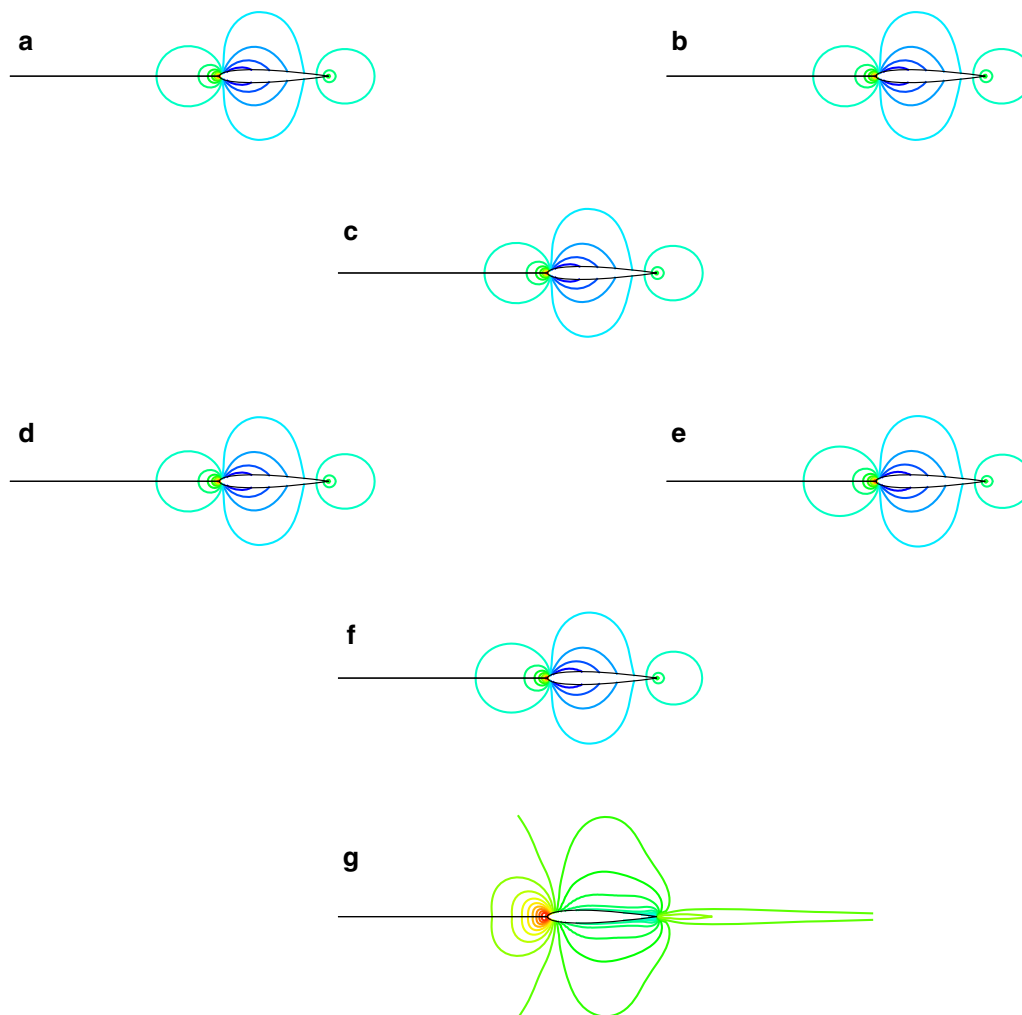


Fig. 10 Pressure contours for simulations of inviscid flow around NACA0012 at $Ma = 0.01$. **a** F-Roe scheme. **b** F-Roe2 scheme. **c** T-D-Roe scheme. **d** T-D-Roe2 scheme. **e** TV-MAS scheme. **f** TV-MAS2 scheme. **g** Roe scheme

tains points of 241 (airfoil) \times 121 (normal) is used for the following computations. The discretization domain extends 19 chord lengths from the airfoil wall, the farfield condition is used at the exterior boundary and the slip wall condition is applied to the airfoil surface. The flow results with several inflow Mach numbers $M_{\text{inf}} = 0.1, 0.01, 0.001$ at a zero-degree angle of attack are investigated to assess the density fix effects. In addition, the flow simulations are conducted by the implicit LU-SGS approach [43] with $CFL=5$ for over 100,000-time iterations, which achieve at least five orders of the density residual reduction (L_2 -norm). Though the preconditioned implicit LU-SGS [23] is a better choice, we still use LU-SGS since we mainly focus on the flux functions.

Figure 9 shows the convergence history of inflow Mach number 0.01 by different schemes. The T-D-Roe serial schemes perform similarly to F-Roe and are not shown in the figure for clarity. We can see clearly in the convergence history that schemes without the energy correction stall after

five orders of residual reduction. The schemes with corresponding corrections can continue with the residual drop.

The results of pressure profiles with inflow Mach 0.01 are plotted in Fig. 10, and density fields of the solutions are presented in Fig. 11. It is important to note that although T-D-Roe, F-Roe, and TV-MAS schemes can obtain accurate pressure flow fields at low speeds, but fail in density fluctuation fields. The schemes with corrections in energy equation can get the accurate density field corresponding to the pressure field. However, in Fig. 11f, the density field of TV-MAS2 seems more diffusive than F-Roe2 and T-D-Roe2, especially in the wake region. This may owe to the inherent dissipation characteristic of HLL Riemann solver solving the pressure system, which is more diffusive than the Roe Riemann solver in nature.

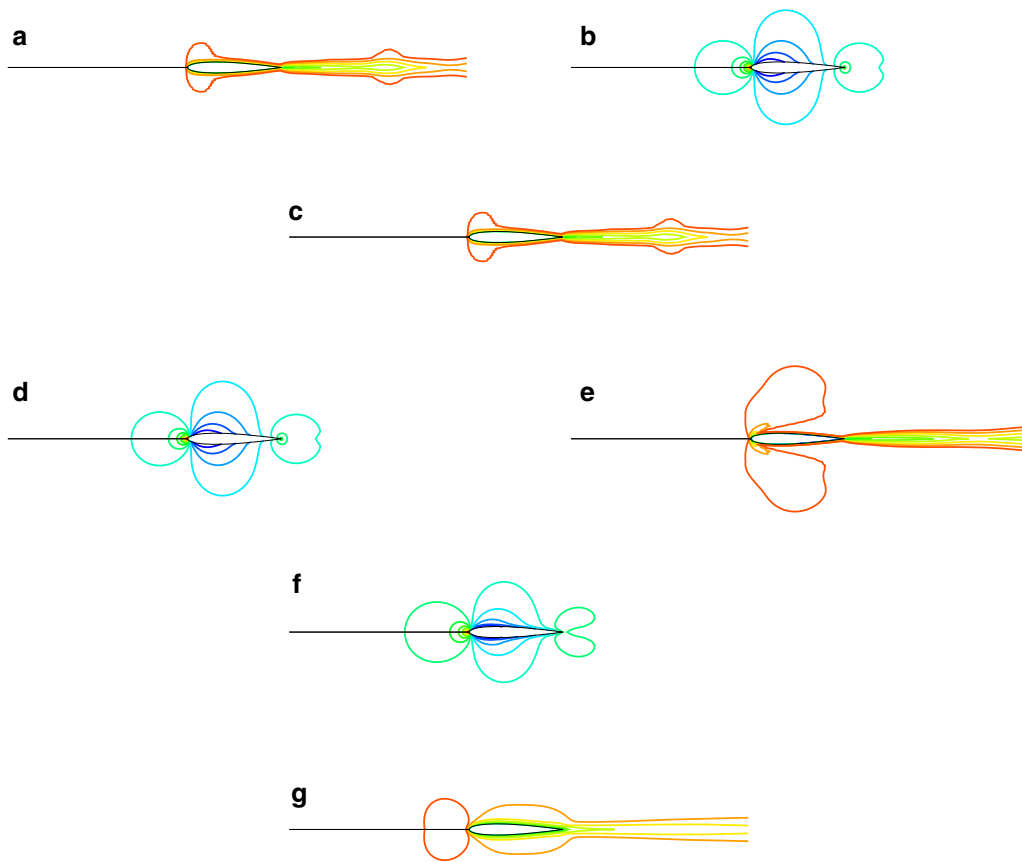


Fig. 11 Density contours for simulations of inviscid flow around NACA0012 at $Ma = 0.01$. **a** F-Roe scheme. **b** F-Roe2 scheme. **c** T-D-Roe scheme. **d** T-D-Roe2 scheme. **e** TV-MAS scheme. **f** TV-MAS2 scheme. **g** Roe scheme

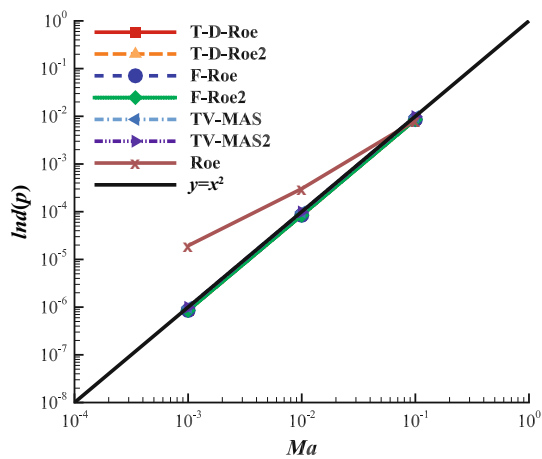


Fig. 12 Comparison of pressure fluctuations computed by different schemes versus inflow Mach number

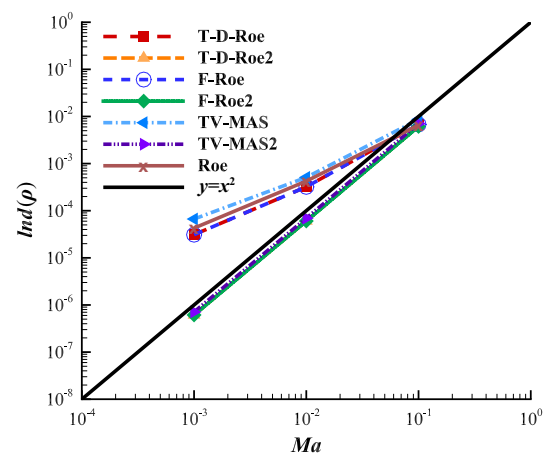


Fig. 13 Comparison of density fluctuations computed by different schemes versus inflow Mach number

Following Ref. [17], we define two fluctuation coefficients as follows

$$Ind(p) = (p_{\max} - p_{\min}) / p_{\max}, \tag{48}$$

$$Ind(\rho) = (\rho_{\max} - \rho_{\min}) / \rho_{\max}. \tag{49}$$

Figure 12 shows pressure fluctuations $Ind(p)$ versus inflow Mach number for inviscid flows over NACA0012 airfoils. Figure 13 shows corresponding density fluctuations $Ind(\rho)$. From these figures, we can draw the conclusions as follows:

- (1) T-D-Roe, F-Roe, and TV-MAS schemes are perfectly consistent with the theoretical asymptotic analysis that the pressure fluctuations scale with the square of the Mach number [7], but fails with the theoretical prediction of density fluctuation.
- (2) T-D-Roe2, F-Roe2, and TV-MAS2 schemes are able to obtain the correct scaling of both pressure and density fluctuations. Thus, they can simulate low Mach number flows more concisely.

6 Conclusion

In this work, we have presented a comprehensive study of the enhancement to a low-speed density fluctuation accuracy problem. The asymptotic analysis has shown the relation of density fluctuation with terms of $\tilde{\rho}\tilde{a}\tilde{U}\Delta U$ in energy equation at low Mach number limit of Roe-type schemes. Applying fix terms in momentum and energy equations at the same time not only can get the expected pressure fluctuations scales of square Mach number and the physical velocity fields, but also can correct the density field into the correct square Mach number scale. An improved TV-MAS scheme, i.e. TV-MAS2, is proposed based on these study. Unsteady Gresho vortex flow, double shear-layer, low Mach number flows over an inviscid cylinder and the NACA0012 airfoil show that energy enhancement terms effectively obtain the expected square of Mach number scaling of density fluctuations, which is in good agreement with corresponding asymptotic analysis. In summary, the energy correction is recommended for low-speed enhancement of upwind schemes when using compressible flow solvers.

Acknowledgements The authors would like to acknowledge the support for this work provided by the National Natural Science Foundation of China (Grant 11402016), and all the authors are grateful to the anonymous reviewers for their constructive comments.

References

1. Zheng, X., Zhou, S., Hou, A., et al.: Separation control using synthetic vortex generator jets in axial compressor cascade. *Acta Mech. Sin.* **22**, 521–527 (2006)
2. Xu, G., Jiang, X., Liu, G.: Delayed detached eddy simulations of fighter aircraft at high angle of attack. *Acta Mech. Sin.* **32**, 588–603 (2016)
3. Zheng, W., Yan, C., Liu, H., et al.: Comparative assessment of SAS and DES turbulence modeling for massively separated flows. *Acta Mech. Sin.* **32**, 12–21 (2016)
4. Fang, J., Lu, L.-P., Shao, L.: Heat transport mechanisms of low Mach number turbulent channel flow with spanwise wall oscillation. *Acta Mech. Sin.* **26**, 391–399 (2010)
5. Turkel, E.: Preconditioning techniques in computational fluid dynamics. *Annu. Rev. Fluid Mech.* **31**, 385–416 (1999)
6. Weiss, J., Smith, W.: Preconditioning applied to variable and constant density flows. *AIAA J.* **33**, 2050–2057 (1995)
7. Guillard, H., Viozat, C.: On the behaviour of upwind schemes in the low Mach number limit. *Comput. Fluids* **28**, 63–86 (1999)
8. Roe, P.L., Pike, J.: Efficient construction and utilisation of approximate Riemann solutions. In: *Computing Methods in Applied Sciences and Engineering*, VI, North Holland, 499–518 (1984)
9. Boniface, J.-C.: Rescaling of the Roe scheme in low Mach-number flow regions. *J. Comput. Phys.* **328**, 177–199 (2017)
10. Li, X.-S., Gu, C.-W.: Mechanism of Roe-type schemes for all-speed flows and its application. *Comput. Fluids* **86**, 56–70 (2013)
11. Li, X., Gu, C.: An all-speed Roe-type scheme and its asymptotic analysis of low Mach number behaviour. *J. Comput. Phys.* **227**, 5144–5159 (2008)
12. Li, X.-S., Gu, C.-W., Xu, J.-Z.: Development of Roe-type scheme for all-speed flows based on preconditioning method. *Comput. Fluids* **38**, 810–817 (2009)
13. Thornber, B.J.R., Drikakis, D.: Numerical dissipation of upwind schemes in low Mach flow. *Int. J. Numer. Methods Fluids* **56**, 1535–1541 (2008)
14. Rieber, F.: A low-Mach number fix for Roe's approximate Riemann solver. *J. Comput. Phys.* **230**, 5263–5287 (2011)
15. Fillion, P., Chanoine, A., Dellacherie, S., et al.: FLICA-OVAP: a new platform for core thermohydraulic studies. *Nucl. Eng. Des.* **241**, 4348–4358 (2011)
16. Li, X.-S.: Uniform algorithm for all-speed shock-capturing schemes. *Int. J. Comput. Fluid Dyn.* **28**, 329–338 (2014)
17. Qu, F., Yan, C., Sun, D., et al.: A new Roe-type scheme for all speeds. *Comput. Fluids* **121**, 11–25 (2015)
18. Sun, D., Yan, C., Qu, F., et al.: A robust flux splitting method with low dissipation for all-speed flows. *Int. J. Numer. Methods Fluids* **84**, 3–18 (2016)
19. Liou, M.-S., Steffen, C.J.: A new flux splitting scheme. *J. Comput. Phys.* **107**, 23–39 (1993)
20. Liou, M.S.: A sequel to {AUSM:AUSM}⁺. *J. Computat. Phys.* **129**, 364–382 (1996)
21. Liou, M.: A sequel to AUSM, part II: AUSM+-up for all speeds. *J. Comput. Phys.* **214**, 137–170 (2006)
22. Shima, E., Kitamura, K.: Parameter-free simple low-dissipation AUSM-family scheme for all speeds. *AIAA J.* **49**, 1693–1709 (2011)
23. Kitamura, K., Shima, E., Fujimoto, K., et al.: Performance of low-dissipation euler fluxes and preconditioned LU-SGS at low speeds. *Commun. Comput. Phys.* **10**, 90–119 (2011)
24. Shima, E., Kitamura, K.: New approaches for computation of low Mach number flows. *Comput. Fluids* **85**, 143–152 (2013)
25. Yao, S.B., Sun, Z.X., Guo, D.L., et al.: Numerical study on wake characteristics of high-speed trains. *Acta Mech. Sin.* **29**, 811–822 (2013)
26. Guo, D., Shang, K., Zhang, Y., et al.: Influences of affiliated components and train length on the train wind. *Acta Mech. Sin.* **32**, 191–205 (2016)
27. Xiao, Z., Fu, S.: Studies of the unsteady supersonic base flows around three afterbodies. *Acta Mech. Sin.* **25**, 471–479 (2009)
28. Qu, F., Yan, C., Sun, D.: Investigation into the influences of the low speed's accuracy on the hypersonic heating computations. *Int. Commun. Heat Mass Transf.* **70**, 53–58 (2016)
29. Qu, F., Sun, D., Shi, Y., et al.: Investigation into the influences of the low speeds' accuracy on RANS simulations. In: *21st AIAA International Space Planes and Hypersonics Technologies Conference*, Xiamen, China, 1–14 (2017)
30. Zha, G., Bilgen, E.: Numerical solutions of Euler equations by using a new flux vector splitting scheme. *Int. J. Numer. Methods Fluids* **17**, 115–144 (1993)
31. Toro, E.F., Vazquez-Cendon, M.E.: Flux splitting schemes for the Euler equations. *Comput. Fluids* **70**, 1–12 (2012)
32. Qu, F., Yan, C., Yu, J., et al.: A new flux splitting scheme for the Euler equations. *Comput. Fluids* **102**, 203–214 (2014)

33. Kapen, P.T., Tchien, G.: An extension of the TV-HLL scheme for multi-dimensional compressible flows. *Int. J. Comput. Fluid Dyn.* **29**, 303–312 (2015)
34. Xie, W., Li, H., Tian, Z., et al.: A low diffusion flux splitting method for inviscid compressible flows. *Comput. Fluids* **112**, 83–93 (2015)
35. Toro, E.F.: *Riemann Solvers and Numerical Methods for Fluid Dynamics*. Springer, Berlin (1997)
36. Sun, M., Takayama, K.: An artificially upstream flux vector splitting scheme for the Euler equations. *J. Comput. Phys.* **189**, 305–329 (2003)
37. Tong, B.G., Kong, X.Y., Deng, G.H.: *Gas Dynamics*, 2nd edn. Higher Education Press, Beijing (2012). (in Chinese)
38. Gresho, P.M.: On the theory of semi-implicit projection methods for viscous incompressible flow and its implementation via a finite element method that also introduces a nearly consistent mass matrix. Part 1: theory. *Int. J. Numer. Methods Fluids* **11**, 620–687 (1990)
39. Gresho, P.M., Chan, S.T.: On the theory of semi-implicit projection methods for viscous incompressible flow and its implementation via a finite element method that also introduces a nearly consistent mass matrix. Part 2: implementation. *Int. J. Numer. Methods Fluids* **11**, 621–659 (1990)
40. Gottlieb, S.: On high order strong stability preserving Runge–Kutta and multi step time discretizations. *J. Sci. Comput.* **25**, 105–128 (2005)
41. Ishiko, K., Ohnishi, N., Sawada, K.: Implicit LES for Two-Dimensional Turbulence Using Shock Capturing Monotone Scheme. In: 44th AIAA Aerospace Sciences Meeting and Exhibit, Reno, Nevada, 1–12 (2006)
42. Kitamura, K., Hashimoto, A.: Reduced dissipation AUSM-family fluxes: HR-SLAU2 and HR-AUSM+–up for high resolution unsteady flow simulations. *Comput. Fluids* **126**, 41–57 (2016)
43. Yoon, S., Jameson, A.: Lower-upper symmetric-Gauss-Seidel method for the Euler and Navier-Stokes equations. *AIAA J.* **26**, 1025–1026 (1988)